Shahid Beheshti University

Sustainable Earth Trends

Journal homepage: http://sustainearth.sbu.ac.ir

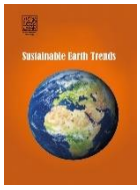

Delineating the impact of climate change on precipitation and groundwater level fluctuations in a semi-arid region of Iran

Elyas Reyhani[a], Seyyed Javad Sadatinejad[a*], Hossein Yousefi[a], Mohammad Mirzavand[a]

[a] School of Energy Engineering and Sustainable Resources, College of Interdisciplinary Science and Technology, University of Tehran, Tehran, Iran

ABSTRACT

In this study, the impacts of climate change on Kashan's groundwater resources were assessed by utilizing outputs from general circulation models (GCMs) and downscaled precipitation data using the SDSM model. For downscaling, the CanESM2 model was applied under the RCP2.6, RCP4.5, and RCP8.5 scenarios to determine precipitation values for future periods. Subsequently, we developed a groundwater model of the aquifer in both steady-state and transient modes using the MODFLOW code within the GMS modeler, based on the hydrological and hydrogeological conditions of the Kashan aquifer. The results of climate downscaling under the CanESM2 model in two scenarios indicated that precipitation percentages during the simulated period of the aquifer (2017-2023) under the RCP2.6, RCP4.5, and RCP8.5 scenarios were 1.17%, 11.77%, and 14.01%, respectively. The reduced precipitation percentages in the climate scenarios of the aquifer model and the magnitude of changes in the water table level for the three scenarios were estimated over 83-time steps. The changes in the water table level during the base period (2016) indicated a decrease of 0.069 m, 0.75 m, and 0.78 m compared to the previous seven-year simulation (2016-2023) at the last time step in the RCP2.6, RCP4.5, and RCP8.5 scenarios, respectively. In light of these climate changes, climate parameter alterations directly correlate with recharge, which could be managed through appropriate water table exploitation practices. Such management necessitates a robust program to compensate for reservoir depletion and mitigate further intensification of water table decline in the area.

ARTICLE INFO

Keywords:
Climate change
SDSM
Groundwater resources
Kashan aquifer
MODFLOW

Article history:
Received: 12 October 2024
Accepted: 23 November 2024

*Corresponding author
E-mail address:
jsadatinejad@ut.ac.ir
(S.J. Sadatinejad)

Citation:
Reyhani, E. et al., (2026). Delineating the impact of climate change on precipitation and groundwater level fluctuations in a semi-arid region of Iran, *Sustainable Earth Trends:* 6(1), (8-22).

DOI: 10.48308/set.2024.237400.1079

1. Introduction

As one of the factors contributing to reduced precipitation due to climate change, it has an adverse effect on groundwater resources (Çelik, 2015). The response of groundwater resources to climate change occurs directly through flux exchange with lakes and wetlands (Yidana et al., 2019; Cui et al., 2020; Bordbar et al., 2023; Najafi et al., 2023). Reduced atmospheric precipitation, excessive exploitation of groundwater resources, and inappropriate cultivation patterns have led to a critical situation for groundwater resources, with groundwater levels exhibiting a decreasing trend in most aquifers (Kowsar, 2006; Mirzavand et al., 2025). Iran is characterized by arid conditions with minimal atmospheric precipitation. A comparison of the average annual precipitation in dry areas worldwide, estimated at 860 mm, with that of Iran, estimated at 250 mm, reveals that Iran receives less than one-third of the average annual precipitation found globally (Brouyère et al., 2004). The Kashan Plain Aquifer in central of Iran has been investigated in this study. The Kashan Plain Aquifer has experienced a significant decline in groundwater quality over the past decades due to salinization (average of EC in KPA in 1965 to 2017 has changed from 5,600 to 26,000 µmohs/cm, respectively). Kashan is one of the major cities in central of

Iran next to Great Kavir. The main source of water for all uses in the Kashan area is groundwater (Mirzavand et al., 2020). Scientific research indicates a rapid increase in greenhouse gas emissions, resulting in elevated global average temperatures and associated side effects. Following the industrial revolution, atmospheric CO_2 concentration has increased by up to 30%, with predictions suggesting a doubling of this concentration within the next 100 years. The Earth's climate is influenced by various factors, including cloudiness, surface energy flows, albedo, radiation, and human activities (Busuioc et al., 2006). Wilby et al. (1998) conducted a study comparing five different models for downscaling data obtained from general circulation models, including the WGEN method and two stochastic C-cric and B-cric methods developed using artificial neural networks for precipitation downscaling. They utilized outputs from HadCM3 climate model in their research. Their findings revealed advantages and disadvantages associated with each model concerning various parameters (Wilby et al., 1998). Rayne et al. (2001) simulated groundwater resources in Sturgeon Bay city, Wisconsin, USA, and determined the recharge areas for freshwater wells in the region. Using the MODFLOW model, they calibrated groundwater simulations in both steady-state and transient modes, concluding that implementing the model in transient mode yielded greater efficiency. Their analysis indicated that the recharge areas for wells were located approximately 10 km north and 7 km south of the city, with a travel time of less than one year from the recharge areas to all wells (Rayne et al., 2001). Khan et al. (2006) compared uncertainty in maximum and minimum daily precipitation in northern Canada, reporting better efficiency of the SDSM model compared to the LARS-WG model (Khan et al., 2006). In a related study, Chu et al. (2010) assessed the performance of the SDSM model in simulating various climatic variables, including temperature, evaporation, precipitation, and extreme precipitation and temperature events, in meteorological stations located within river watersheds in China. They found that the SDSM model exhibited proficiency in downscaling precipitation, temperature, and evaporation (Chu et al., 2010). Furthermore, Wang et al. (2014) introduced a novel package for simulating groundwater flows utilizing MODFLOW in sloping-free aquifers. This package proved to be well-suited for predicting hydraulic heads along the vertical profile of aquifers characterized by slopes lower than 0.50 (Wang et al., 2014).

Similarly, Wu et al. (2015) investigated climate change dynamics by employing a variable diffusion coefficient model to assess future flood risks in Beijing, China. Utilizing three diffusion scenarios based on GCM models for simulations, they concluded that while the VIC model showed promise for flood simulation, significant uncertainty persisted when using GCM tools and diffusion scenarios to predict future flood risks (Wu et al., 2015).

Ahmad et al. (2017) conducted simulations of groundwater in the Dera Ghazi Khan Area of Pakistan using the MODFLOW environment, concluding that maximizing surface water or flood usage leads to an increased level of groundwater resources (Ahmad et al., 2017). Goodarzi et al. (2019) investigated the impacts of climate change on crop water requirements and regional cropping patterns, utilizing two climate change scenarios and combinations of 20 GCM models. Various models, including CROPWAT, MODFLOW, and statistical models, were employed to evaluate these impacts. The results indicated that in the future period (2017-2046), temperatures are projected to increase across all months of the year at all stations. The average annual precipitation is expected to decline at Isfahan, Tiran, Flavarjan, and Lenj stations for RCP 4.5 and RCP 8.5 scenarios, with percentages ranging from 10.5% to 31.5%. Additionally, the average increase in evapotranspiration for RCP 4.5 and RCP 8.5 scenarios is approximately 2.5% and 4.1%, respectively. These findings suggest that climate change could significantly impact water resources consumption (Goodarzi et al., 2019; Diancoumba et al., 2023), Most of the studies have employed modeling-based methodologies with a focus on groundwater use, primarily in agricultural areas (Arshad et al., 2022; Ashraf et al., 2022).

Therefore, this study utilizes an integrated modeling framework consisting of MODFLOW applications to investigate groundwater changes in the context of projected climate change impacts on groundwater resources in the Kashan Aquifer. Additionally, we propose several adaptation options to mitigate the diminishing groundwater resources.

2. Material and methods

2.1. Study Area

The Kashan plain aquifer is situated within longitude coordinates of 50°54'39" to 52°06'03" and latitude coordinates of 33°36'36" to 34°30'06" (Fig. 1). This watershed is bounded by Qom to the north and northwest, Muteh to the southwest, Natanz to the south, and Namak Lake to the east. It covers an area of 6950 km², with 3551 km² in highlands and 3399 km² in plains. According to the De Martonne method, the Kashan Plain is classified as a dryland with a drought index of 4.8. Conversely, the southern mountainous regions of Kashan exhibit a specific climate categorized as semi-arid according to the De Martonne classification. The synoptic station at Kashan Airport is positioned at an east longitude of 51°27' and a north latitude of 33°59', with an elevation above mean sea level of 982.3 meters.

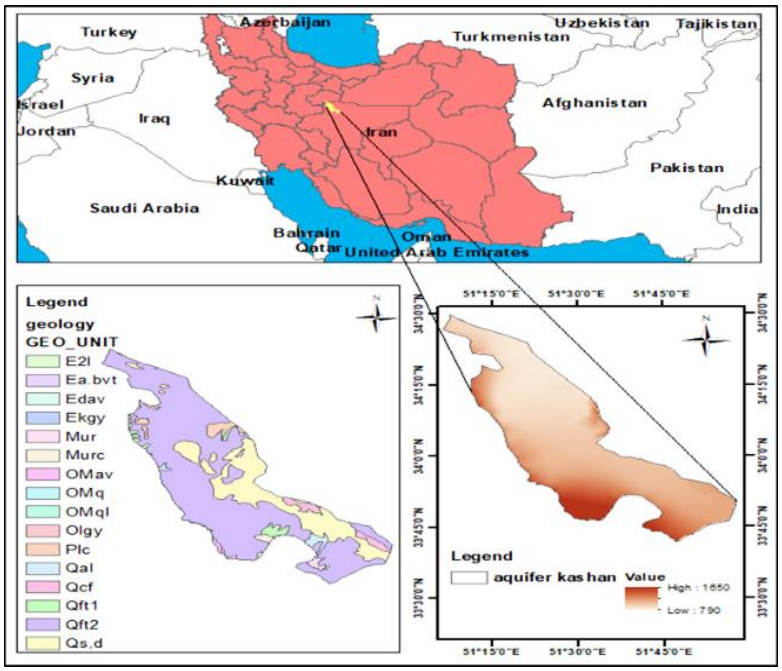

Fig. 1. Study area location.

2.2. Conceptual Model

In this study, simulating three-dimensional unsteady groundwater necessitates comprehensive information and a detailed description of the groundwater system. This database encompasses hydraulic parameters (such as hydraulic conductivity, specific yield, and transmissivity), budget components (including recharge from rivers, precipitation, well pumping, evapotranspiration, and return water from irrigation), geological data (such as digital elevation model (DEM) layers and aquifer thickness), and boundary conditions (comprising impermeable boundaries and general or constant heads). The conceptual model of the study area underwent a transition from continuous to discrete limits in the numerical model, being gridded in a cell-centered format with dimensions of 500 meters by 500 meters. The number of cells in the direction of the x-axis is equal to 189 and for the y-axis is equal to 180. Expanding an accurate conceptual model holds significant importance in the numerical modeling process of groundwater flows. However, designing a conceptual model is complex and time-consuming, often hindered by the inaccuracy and limited availability of accessible data, particularly in developing countries. The proposed method encompasses six steps. Step 1 involves the collection of all necessary data and information, resulting in the output titled "controlled observations" or conceptual model version 00. Due to its crucial role, this step requires meticulous evaluation. Step 2 determines the geometry of the aquifer, yielding conceptual model 01 as the output. Step 3 involves determining hydraulic properties, resulting in conceptual model 02. Step 4 evaluates surface and subsurface interactions and internal/external groundwater flows, producing conceptual model version 03. Step 5 combines the outputs of the previous

steps to provide the final conceptual model, assessing the accuracy level of the conceptual model and the annual groundwater balance (Izady et al., 2014). Input MODFLOW data are obtained from GMS. The modularity of the program refers to its structure comprising separate and independent segments, each assigned with a specific task. These modules are organized to simulate different parts of the hydrological system. The methodology framework of this research is presented in Fig. 2.

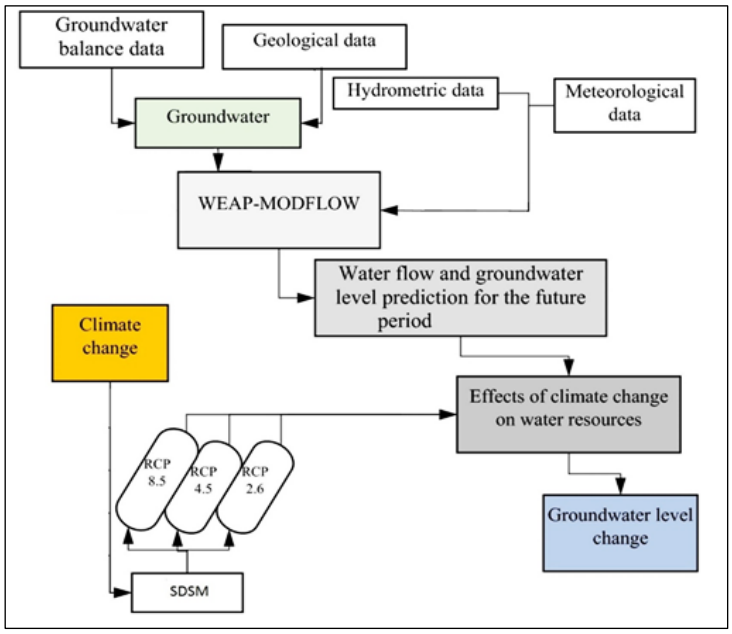

Fig. 2. Methodology framework of the research.

2.3. Data gathering

Basic data and information were collected and imported into GMS to develop the groundwater model. This information is presented in different sections.

Hydrological parameters: The hydraulic conductivity of the Kashan aquifer has been extracted from available documents and studies available at the Kashan Regional Water Organization.

Piezometric and extraction wells: This package includes 43 piezometer wells (observation wells) and 2007 pumping wells and qanats. Fig. 3 illustrates the well package of the Kashan aquifer. there are 2007 wells in the Kashan basin, 2007 of which with an annual extraction of 318 Mm^3 are located in the Kashan aquifer. Also, 26.5 Mm^3 of the groundwater of Kashan. Data of the 43 observation wells were applied to simulate the steady-state groundwater model.

Water withdrawal information and Recharge package: Groundwater recharge, a crucial component of the water budget, was determined using the MODFLOW model. Utilizing the extracted recharge data and accumulation of deviations from average rainfall (AAR) in MATLAB software, an appropriate regression equation was derived. This study operates under the assumption that the relationship between rainfall and recharge remains consistent despite changes in climate. The primary sources of recharge for the Tehran aquifer include Groundwater inflow, precipitation, runoff, local rivers, and return from domestic water supply (Including drinking, industrial, and agricultural water). Conversely, the aquifer experiences discharge through groundwater outflow, evapotranspiration, and discharge from agricultural, industrial, and drinking water wells, as well as springs and qanats. The water balance of the aquifer is presented in Table 1 (Mahjouri et al., 2005). Mahjouri et al. (2005), simulated the Kashan aquifer using the PMWIN model. The water balance of this aquifer was estimated based on available data, including discharge from agricultural wells, monthly infiltration rates from channels and rivers, and agricultural return flow (Mahjouri et al., 2005). The recharge package was derived from a land use map and information on recharge rates for each land use category, including agricultural, industrial, urban, rangelands, and Playa areas. By integrating the

land use map with groundwater recharge information, the model generated a recharge map as input. Fig. 4 illustrates the recharge package of the Kashan aquifer. Considering the depth of the groundwater level in the region, which is more than 9 m, evaporation does not play a role in the groundwater balance in the region.

Boundary conditions: To build the numerical model, different boundary conditions must be defined. In the case of Kashan aquifer, fixed-head boundary conditions in specific head and general head were applied to describe boundary conditions. Boundary conditions in the study area were simulated using general head.

Table 1. The Water Balance of Kashan Aquifer (Mahjouri et al., 2005).

Water Balance Variable	Discharge (MCM)	Recharge (MCM)
Inflow at the boundaries	-	118.04
Precipitation	-	53.12
Infiltration from stream and canals and dry parts of qanats	-	50
Infiltration from absorption wells	-	20
Agricultural return flow	-	110
Outflow at the boundaries	0.73	-
Discharge from wells and springs	318	-
Discharge from qanats	26.5	-
Change in groundwater volume	5.93	-

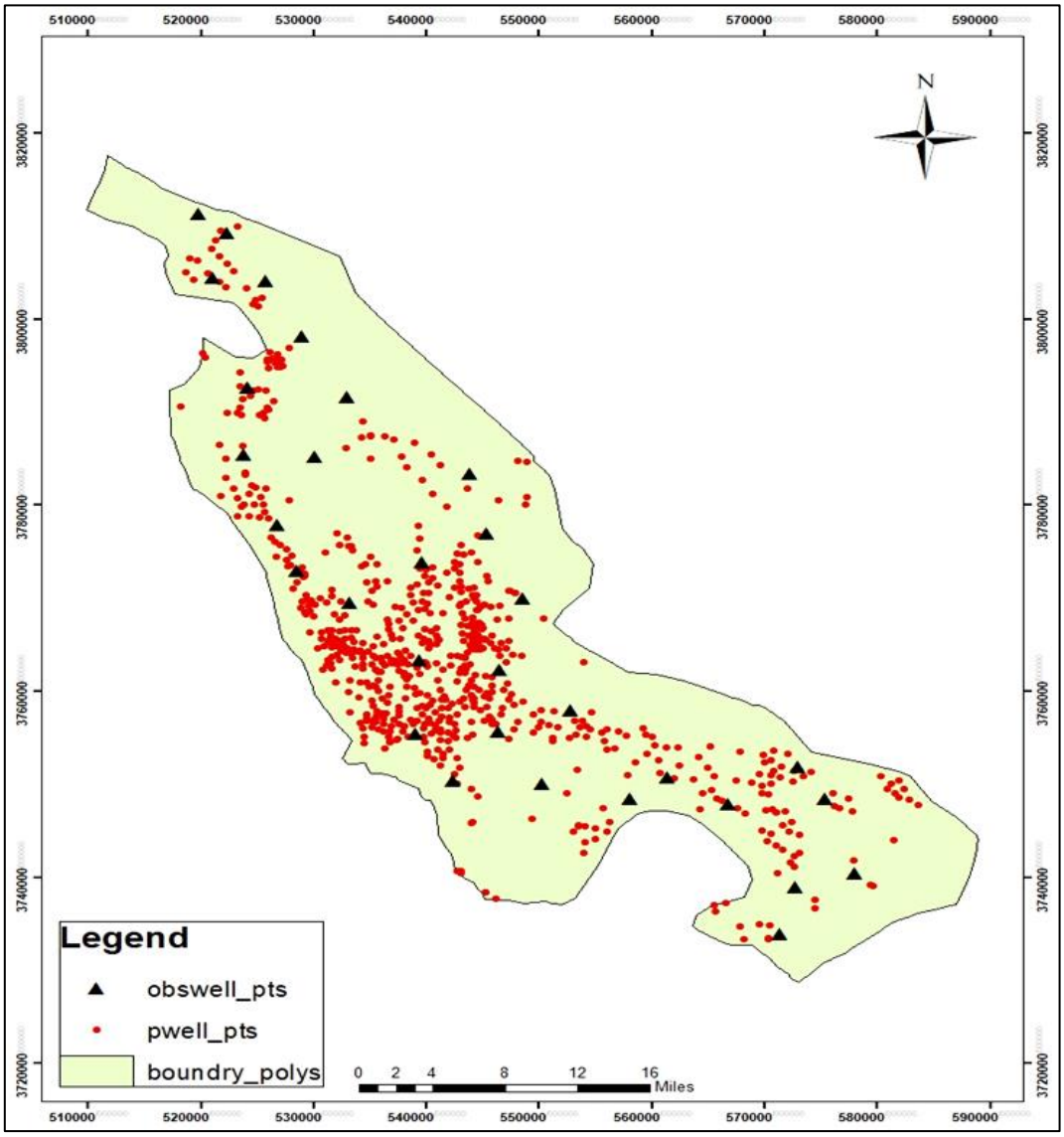

Fig. 3. Well package of Kashan aquifer (exploitation wells (red circles) and piezometric wells (black triangles)).

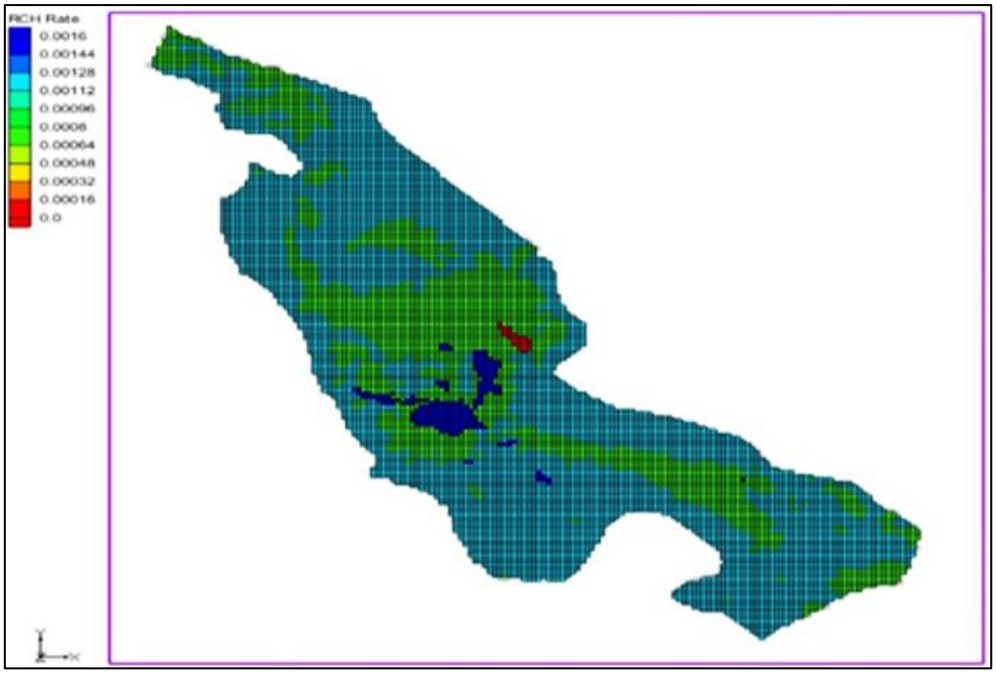

Fig. 4. Recharge package of Kashan aquifer.

2.4. Models

2.4.1. SDSM Model

The SDSM model is a stochastic weather generator capable of statistically downscaling daily weather series through the execution of six discrete functions. The purpose of each function is outlined below:

Quality Control and Data Transformation: This function involves checking the quality, accuracy, and completeness of the input dataset by identifying gross data errors and specifying missing data codes and outliers before model calibration. Additionally, it offers the option to transform predictors and/or predicted data prior to model calibration using transformations such as logarithmic, power, inverse, lag, and binomial transformations.

Screening of Downscaling Predictor Variables: This function aims to identify large-scale predictor variables (e.g., NCEP) that are significantly correlated with observed station data (predictands). Various indicators such as partial correlation, correlation matrix, explained variance, P-value, histograms, and scatter plots are utilized in SDSM to select suitable predictors from a group of atmospheric predictors. Screening of predictors is crucial as it determines the character of the downscaled climate scenario. However, multiple collinearities between predictor variables can occur, posing a challenge during screening. This issue should be addressed during predictor selection.

Model Calibration: The model calibration function utilizes a user-specified predicted set along with the screened predictor variables to compute the parameters of multiple regression equations via an optimization algorithm (either dual simplex or ordinary least squares) for model calibration. Before calibration, the user must specify the model structure (e.g., monthly, annual, or seasonal sub-models) and whether the process is unconditional or conditional.

Weather Generator: This function generates ensembles of synthetic daily weather series from observed (or re-analysis) atmospheric predictor variables. It allows verification of the calibrated model using independent data of observed predictors and produces artificial time series for present climatic conditions. The user specifies the period of record to be synthesized and the desired number of ensemble members. The stochastic component of SDSM enables the generation of up to 100 ensembles of data with the same statistical characteristics but varying on a day-to-day basis.

Scenario Generation: The scenario generator function produces ensembles of synthetic daily weather series from GCM-derived atmospheric predictor variables, either for present or future climate, using the statistical relationship established by the model calibration function. Scenario generation is similar to weather generation, but input files for scenario

generator need not be the same length as those used to obtain regression weights during calibration.

Diagnostic Testing/Analysis: This function allows comparison of the statistical characteristics of both observed and synthetic data using options such as 'Summary Statistics' and 'Compare Results' in SDSM. This comparison aids in determining the effect of spatial downscaling, with summary statistics summarizing the results of both observed and simulated data, and compare results enabling the plotting of the result of summary statistics (Wilby and Wigley, 1997) .

Introduction of CanESM2 Model: In this research, the CanESM2 model, based on the fifth report of the IPCC, is utilized for simulating the precipitation climate parameter. The rationale for selecting this model lies in its widespread application in climate change research and the ease of access to its information (Table 2). The CANESM2 general circulation model, featured in the fifth report of the IPCC, is utilized in three scenarios: RCP2.6, RCP4.5, and RCP8.5, as outlined in Table 3. This model is grid-based, comprising 128×64 cells (longitude × latitude), with a resolution of 2.8125° for both longitude and latitude. The NCEP data span from 1961 to 2005. Additionally, data for the RCP2.6, RCP4.5, and RCP8.5 scenarios are selected from 2006 to 2100.

Downscaling of Climate Parameters: In this section, we utilize the RCP2.6, RCP4.5, and RCP8.5 climate scenarios of the SDSM4.2 model to downscale precipitation climate parameters based on the outputs of the CanESM2 model. Following the calibration and validation of the model, each scenario spanning from 2010 to 2039 is compared with the baseline period. The downscaling process for the Kashan station is detailed subsequently. Initially, the SDSM model is employed to select predictors for the climate parameters. Six final parameters with large-scale significance are chosen for precipitation, and the results of these selected final predictors are presented in Table 4 (Abdo et al., 2009).

Table 2. GCM Models based on 4th Report of IPCC.

Report	Centre	Model	Resolution
AR5	Canadian Center for Climate Modeling and Analysis	CanESM2	(2.78˚ lat x 2.81˚ long)

Table 3. Climate Scenario of 5th Report.

Scenario	Designing Country and Institute	Key Hypothesis
RCP8.5	The MESSAGE modeling team and the International Institute for Applied Systems Analysis (IIASA) in Austria.	Without mitigation efforts and climate change policies, the Earth's climate will persist along a trajectory of propagation, ultimately resulting in a radiative forcing of 8.5 watts per square meter by 2100. By that time, the concentration of carbon dioxide is projected to reach 1,000 ppm, with this trend expected to continue increasing.
RCP4.5	The MiniCAM modeling group and the Joint Global Change Research Institute (JGCRI) located in the northwest of the Pacific Ocean.	The radiative forcing resulting from greenhouse gases will remain constant at 4.5 watts per square meter until 2100.
RCP2.6	The IMAGE modeling team from the Netherlands Environmental Assessment Agency.	The radiative forcing is projected to reach 3.1 in the middle of the century, decreasing to 2.6 watts per square meter by 2100. Achieving this reduced level of radiative forcing necessitates a significant decrease in greenhouse gases.

Table 4. List of predictor variables in NCEP reanalysis data.

S.N	Predictor variables	Description of predictor variables
1	pmslpgl	Mean sea level pressure
2	p1_vgl	1000hPa Meridional wind component
3	p1_zgl	1000hPa Relative vorticity of wind
4	prcpgl	Total precipitation
5	pshumgl	Surface specific humidity
6	ptempgl	Mean temperature at 2m

After validating the data, daily statistics from the meteorological organization were chosen for downscaling the precipitation parameters of the Kashan synoptic station over a period of 35 years. In this paper, two graphical and statistical methods, namely R^2 (Eq. 1) and RMSE (Eq. 2), are employed to assess the model's efficiency. A value closer to 1 indicates a stronger relationship between the data. The estimation methods for these two parameters are as follows:

$$R^2 = \left[\frac{\frac{1}{n}\sum_{n=1}^{n}(S_i-S)(O_i-O)}{\sigma_s-\sigma_o}\right]^2 \quad \text{(Eq.1)}$$

$$RMSE = \left[\frac{1}{N}\sum_{n=1}^{N}(Si-Oi)^2\right]^{1/2} \quad \text{(Eq.2)}$$

Where O_i stands for observational data, S_i stands for estimated data, and σ stands for variance.

MODFLOW Model: Toth pioneered the use of modeling methods for groundwater flow in the drainage of a small watershed in 1963. In subsequent years, particularly in 1970, 1971, and 1972, Toth developed a hierarchical system for groundwater flows at local, regional, and inter-regional scales. Computer models, including three-dimensional limited models from the United States Geological Survey and the MODFLOW model from the United States Geological Survey (McDonald and Harbaugh, 1988), were utilized. Harbaugh et al. further enhanced the MODFLOW models, updating them to MODFLOW2000 and MODFLOW2005 in 2000 and 2005, respectively, to accommodate input hydrological data and improve simulation capabilities (Zhou and Li, 2011) .
The general equation of groundwater balance is given in Eq. 3.

$$\Delta V=Q_{in}-Q_{out} \quad \text{(Eq.3)}$$

Where Q_{out} represents factors affecting aquifer discharge, and Q_{in} represents factors affecting aquifer recharge. Changes in the volume of water storage (ΔV) in the aquifer are given in Eq. 4.

$$\Delta V=\pm SA\Delta h \quad \text{(Eq.4)}$$

Where S and A are Special discharge (%), and Aquifer area (Km^2), respectively.
The GMS numerical model is based on the groundwater equation of motion. So that the three-dimensional groundwater movement is solved by the partial differential equation (Eq. 5) using the finite difference method and on the basis of the continuum equation.

$$\frac{\partial}{\partial x}\left|kxx\frac{\partial h}{\partial x}\right| - \frac{\partial}{\partial y}\left|kyy\frac{\partial h}{\partial y}\right| + \frac{\partial}{\partial z}\left|kzz\frac{\partial h}{\partial z}\right| - W = S_s \quad (5)$$

Where K (m^2/s), H, W, Ss, and T are Hydraulic conduction of a porous environment, potential, Volume Flux in Volumetric Unit - Indicator of recharge and Water Discharge, Special storage of porous materials, and time (Schweizer, 2015). This model has been used in previous hydrological studies (Mastrocicco et al., 2014; Narany et al., 2017; Taie Semiromi and Koch, 2020), respectively.

3. Results and Discussion

3.1. Comparison of observational and simulated data

To validate the large-scale model, precipitation parameters from the previous period were utilized, and their results are depicted in Fig. 5 for the CanESM2 model. Fig. 5 illustrates a diagram showing the difference in levels between simulated and observational data during the baseline period. The months of January, February, September, October, November, and December are considered wet periods of the year, while June and July are considered dry periods. The remaining months are classified as normal.

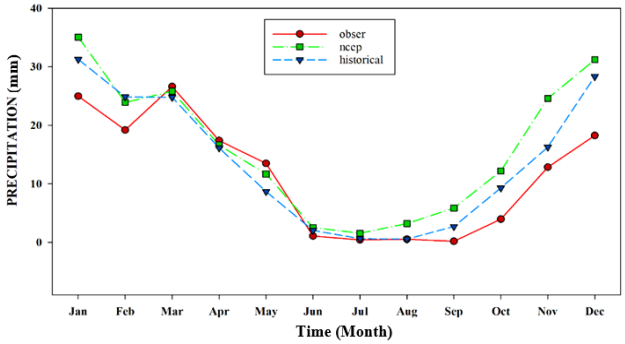

Fig. 5. Comparison of observational and modeled data in the validation stage in the CanESM2 model (1995-2003).

3.2. Calibration of CanEsm2 model

The results of two graphical and statistical methods used to assess the efficiency of CanESM2 are presented in the following section. Model validation is crucial as it demonstrates the model's ability to replicate observational data accurately. Based on the comparison between simulated and observational data depicted in Fig. 5, as well as the statistical evaluations presented in Table 5, it can be concluded that this model is valid and suitable for predicting precipitation parameters from 2010 to 2039. This validation enables more accurate management of water resources and their preservation. Precipitation parameters for the period of 2010-2039 are predicted for the RCP2.6, RCP4.5, and RCP8.5 scenarios using the CanESM2 model. The results are depicted in three curves representing monthly precipitations. As shown in Fig. 6, which illustrates the prediction diagram of precipitation for future periods, it can be observed that February, March, April, October, and September in the RCP2.6 scenario exhibit higher precipitations compared to the other two scenarios. However, the precipitation levels for the other months remain similar across all three scenarios.

Table 5. Calibration of the CanEsm2 model in comparison with observational data (2004 and 2005).

Precipitation		General Circulation Models	
R2	**RMSE**		
0.69	4.5	Historical	CanESM2
0.83	6.3	Ncep	

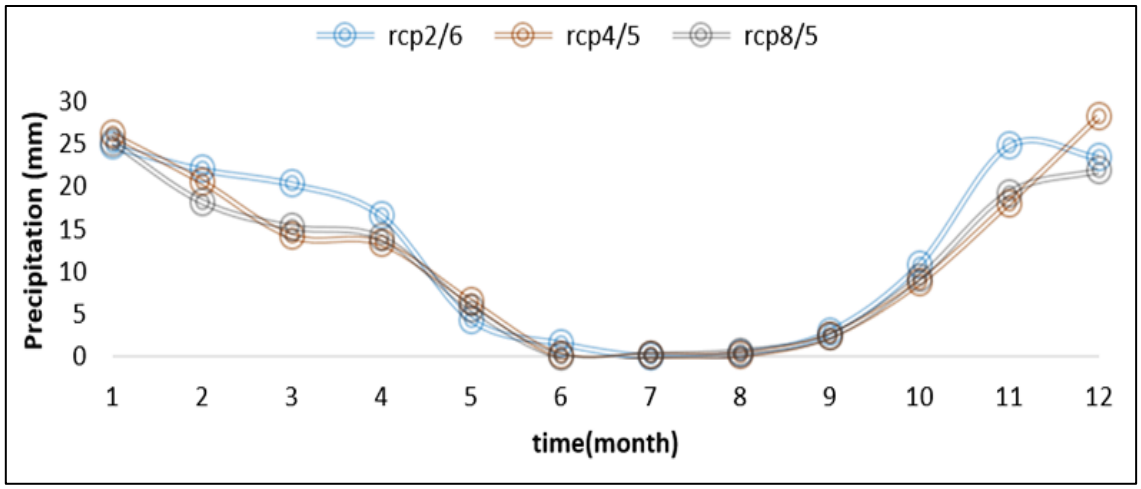

Fig. 6. Data simulated sum monthly of rainfall for basin in during next period (2010-2039).

Fig. 6 displays simulated precipitation data for future periods under three scenarios: RCP2.6, RCP4.5, and RCP8.5. As depicted in the diagram, the RCP2.6 scenario exhibits higher precipitation during spring, summer, and fall compared to the other two simulated scenarios. However, during winter, the RCP4.5 scenario shows higher precipitation levels. Our findings that RCP2.6 exhibits higher precipitation during Spring, Summer, and Fall seasons correspond with studies indicating that low-emission scenarios (e.g., RCP2.6) often result in more localized and intense precipitation events due to reduced radiative forcing. For instance, Knutti and Sedláček (2013) highlight that RCP2.6 generally leads to more equitable precipitation distribution, particularly in mid-latitude regions, due to stabilized temperature gradients and moderated evaporation rates. Similarly, Hempel et al. (2014) note increased seasonal precipitation under RCP2.6 in some regions, particularly during the growing season, which aligns with your spring and summer findings. The higher winter precipitation levels under RCP4.5 in this study agree with research indicating that moderate warming scenarios (e.g., RCP4.5) can intensify the hydrological cycle, especially during winter. This is driven by the increased capacity of a warmer atmosphere to hold and transport moisture, leading to heavier precipitation during cooler months. Collins et al. (2013) discuss similar trends, noting that in scenarios with moderate radiative forcing, winter precipitation is more

pronounced due to enhanced moisture availability and larger-scale atmospheric circulation changes. Studies by Chou et al. (2014) and Watterson et al. (2015) emphasize that the seasonal distribution of precipitation often varies significantly between RCP scenarios, with RCP4.5 typically exhibiting stronger seasonality due to intermediate greenhouse gas concentrations. our observation of distinct seasonal differences, such as higher precipitation under RCP4.5 in winter versus RCP2.6 in other seasons, is consistent with these studies. For additional comparison purposes, Table 6 and Fig. 7 presents the annual climatological sum of observed and simulated rainfall for the next period (2010-2039) across the entire basin. These values illustrate the performance of each method in downscaling rainfall relative to the observed dataset.

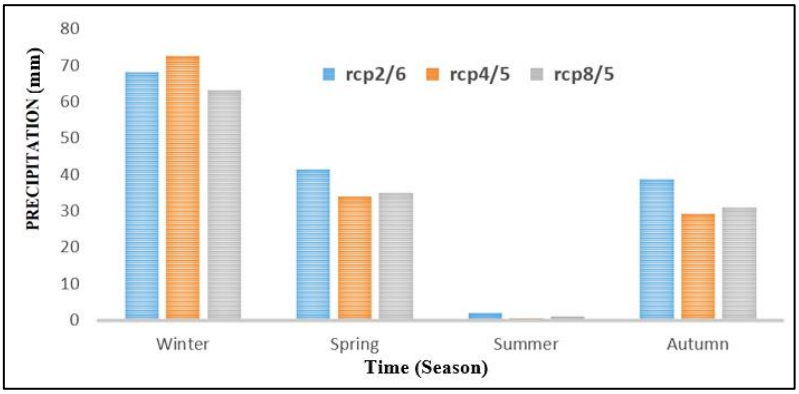

Fig. 7. Observed vs. simulated sum season rainfall graph for basin in during next period (2010-2039).

Table 6. Historical vs. simulated annual climatological means.

N.S	Time Period	Annual (mm)
1	historical	154/037
2	CanESM2 AOGCM RCP 2.6 (2010-2039)	152/222
3	CanESM2 AOGCM RCP 4.5 (2010-2039)	138/901
4	CanESM2 AOGCM RCP 8.5 (2010-2039)	132/439

Based on the outputs of the CanESM2 model, the comparison of precipitation changes between the baseline period and future periods (2010-2039) reveals a reduction of up to 1.17% in the RCP2.6 scenario and up to 11.77% in the RCP4.5 scenario. Notably, precipitation at the Kashan station decreases by up to 14.01% in the RCP8.5 scenario.

3.3. Modeling in transit Conditions

Through steady-state modeling and calibration of parameters for the year 2009, with transient primary components, stress courses were chosen based on available hydrologic data for the area. Consequently, the Kashan aquifer was simulated monthly over 83-time steps, spanning from January 2009 to December 2015. Given that the Kashan aquifer is unconfined, the specific yield coefficient must also be factored into consideration for modeling the transient mode.

3.4. Calibration in transit Condition

During this step, modeling was conducted using non-optimized parameters over 83-time steps, commencing from January 2009 and concluding in December 2015. To calibrate the model, a trial-and-error approach was initially employed for the specific yield. Subsequently, automatic calibration (utilizing the PEST package) was implemented on hydraulic parameters through multiple runs until achieving the highest consistency between estimated and observed values, thus optimizing the model. In the automatic calibration process, the regional model was initially utilized for optimization, with parameters being optimized via pilot points. Fig. 8 illustrates the comparison between the calculated and observed water levels associated with the transient model calibration. This output validates the adequacy of the model calibration. Additionally, Figure 8 displays low error values under transient conditions for both estimated and observed values. This figure demonstrates the suitability of the modeling approach for each time step.

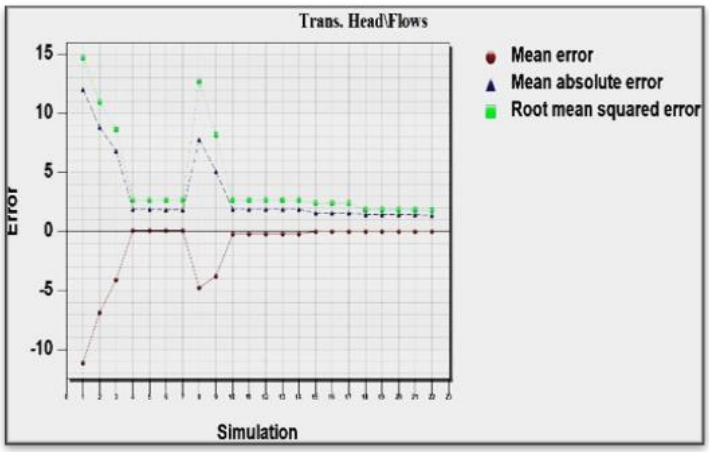

Fig. 8. Diagram and error value of transient condition in quantitative mode.

3.5. Verification of the Model

Verification is conducted to further ensure the efficiency of the model and its predictive capability for data beyond calibration and temporal data. It offers the opportunity to evaluate the reliability of the estimated parameters and the presented model (Gharbia et al., 2015) , The boundary conditions of the model during the verification step encompass the northeast, east, and southeast boundaries, as well as a portion of the western aquifer for recharge, and the northeast border for aquifer evacuation. These conditions are assumed to remain steady-state throughout the estimation period. For verification of the results, a period from January to December 2016 is selected, corresponding to the calibration period. The output of observational errors in the initial time step is depicted in Fig. 9. Fig. 9 demonstrates that the wells possess modeling capacity as a result of optimized parameters during the calibration step. Additionally, test statistics are utilized to indicate high efficiency and verify the model for the period from January 1, 2016, to December 1, 2016. The RMSE, MSE, and ME for this period were calculated as 1.12, 0.62, and -0.25, respectively. Based on these test statistic values, it can be concluded that the presented model exhibits appropriate accuracy.

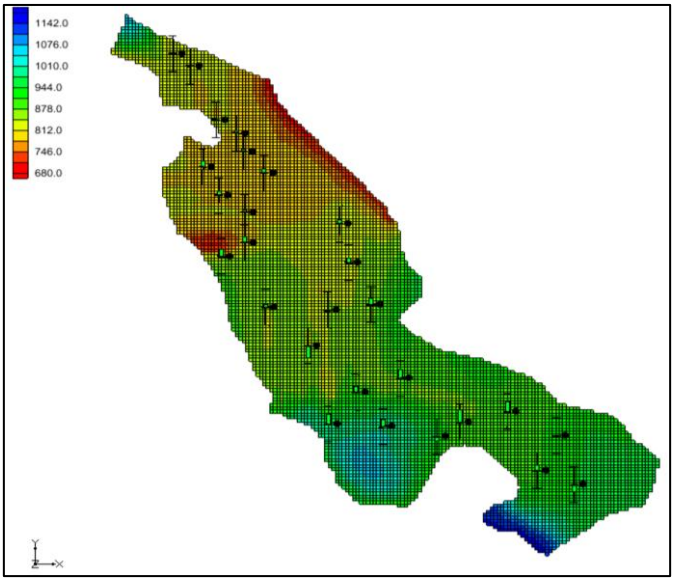

Fig. 9. Error of the model in verification step.

3.6. Simulating future aquifer conditions under the influence of climate change phenomena

The calibrated and validated groundwater model can be utilized for various management and planning studies. The optimized parameters acquired through model calibration are valuable for predicting the aquifer's response to future changes. Simulations were conducted to elucidate how the aquifer would vary in

response to climate change, particularly changes in recharge rates. Monthly precipitation variations over a seven-year period were investigated across different scenarios to simulate the aquifer's condition under the influence of climate change phenomena. The simulation spanned from January 2017 to December 2023, taking into account changes in the water table. Subsequent paragraphs will detail the fluctuations in water levels across different climate scenarios.

Scenario 1: RCP2.6: To assess the impacts of climate change on groundwater resources under scenario RCP2.6, the provided model was updated until the end of 2016. A suitable climate phase was defined to apply the climate scenario in line with the model outputs. In scenario RCP2.6, annual precipitation decreased by -1.17, indicating monthly variations in aquifer discharge. The future simulated period spanned from January 2017 to December 2023, comprising 83 monthly time steps. Assuming constant exploitation of wells in future periods, the average changes in groundwater level were estimated based on the groundwater levels of the baseline period. A reduction of -0.069 meters was observed in the aquifer. Fig. 10 illustrates that groundwater level changes decreases from -0.2 to -5.54.

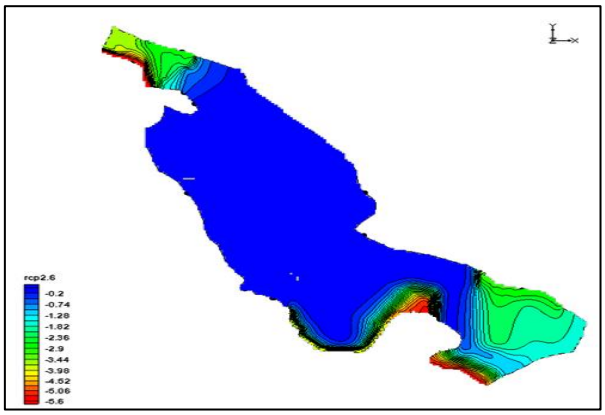

Fig. 10. Groundwater level variation between 2017 and 2023 by applying RCP2.6 scenario.

Scenario 2: RCP4.5: To assess the impacts of climate change on groundwater resources under scenario RCP4.5, the provided model was updated until the end of 2016. An appropriate climate phase was defined for the application of the climate scenario based on the model outputs. In scenario RCP4.5, annual precipitation decreased by -11.17, indicating monthly changes in aquifer discharge. The future simulated period extended from January 2017 to December 2023, with 83 monthly time steps. Assuming constant exploitation of wells in future periods, the average changes in groundwater level were estimated based on the groundwater levels of the baseline period. A reduction of -0.75 meters was observed in the aquifer. Fig. 11 illustrates a reduction in the range of water level change, from -0.33 to -5.54. On the western side, the water level descends to the bed, indicating that wells in the agricultural exploitation area of this region are dry.

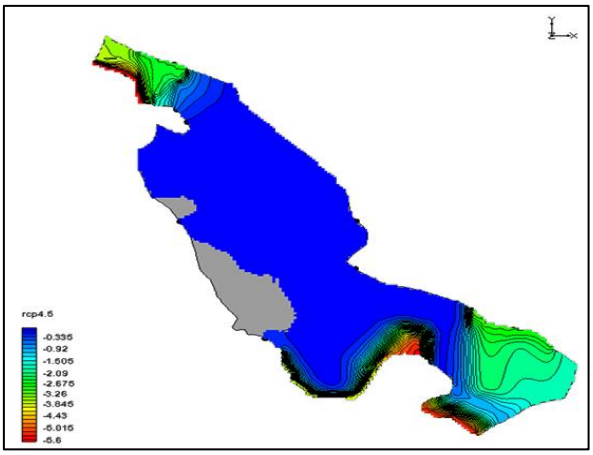

Fig. 11. Groundwater level difference between 2017 and 2023 by applying RCP4.5 scenario

Scenario 3: RCP8.5: To assess the impacts of climate change on groundwater resources under scenario RCP8.5, the provided model was updated until the end of 2016. An appropriate climate phase was defined for the application of the climate scenario with respect to the model outputs. In scenario RCP8.5, annual precipitation decreased by -14.01, indicating monthly changes in aquifer discharge. The future simulated period began in January 2017 and concluded in December 2023, consisting of 83 monthly time steps. Finally, assuming constant exploitation of wells in future periods, the average changes in groundwater level were estimated based on the groundwater levels of the baseline period. A reduction of -0.78 meters was observed in the aquifer. Fig. 12 illustrates a reduction in the range of water level change, from -0.7 to -5.54. Compared to the previous scenario, there is an increase in the areas where the water level reaches the bed.

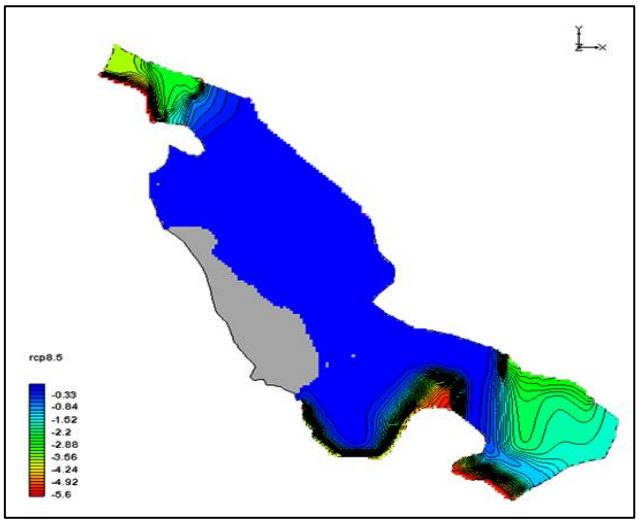

Fig. 12. Groundwater level difference between 2017 and 2023 by applying RCP8.5 scenario.

4. Conclusion

Due to the low spatial resolution of general circulation models, these models cannot provide an accurate approximation for the climate conditions of the study area. Therefore, their output must be downscaled to match the resolution of meteorological stations. With the aim of downscaling temperature and precipitation climate parameters resulting from the CanESM2 model in RCP2.6, RCP4.5, and RCP8.5 scenarios, the SDSM4.2 model was employed. After calibration and verification, the changes in each scenario during the period 2039-2010 were compared to the base period. Downscaling was carried out for the synoptic station of Kashan. The outputs of these two models are summarized for different scenarios. According to the outputs of the CanESM2 model, precipitation changes during the base period compared to the future period decreased by up to 1.17% for the RCP2.6 scenario, up to 11.77% for the RCP4.5 scenario, and eventually up to 14.01% for the RCP8.5 scenario at the Kashan station. An appropriate climate phase was defined for the application of the climate scenario with respect to the outputs. In the RCP2.6, RCP4.5, and RCP8.5 scenarios, annual precipitation reduced by 1.17%, 11.77%, and 14.01%, respectively. These reductions led to changes in aquifer discharge. Finally, assuming constant exploitation of wells in future periods, average changes in groundwater level were estimated based on the groundwater level during the base period. Resource volume was reduced by up to 1392139.10, 13208686.13, and 17171291.97 m2 in the RCP2.6, RCP4.5, and RCP8.5 scenarios, respectively. According to the simulation results and observations and estimations of water surface, it is evident that the proposed model can calibrate the parameters and has an appropriate correlation and estimation errors. Therefore, this model has multiple applications. Climate changes and increased exploitation of groundwater resources have significantly reduced the water table of the Kashan Aquifer. However, determining the weight of each factor of exploitation and climate is an important issue in the management of groundwater resources. The present research indicates that changes in

climate parameters have a direct relationship with recharge, and consequently, appropriate planning and management can mitigate climate change risks and their serious damages.

Acknowledgments

We would also like to thank the reviewers for their insightful comments, which significantly improved the quality of our work. This research received no specific financial support.

References

Abdo, K., Fiseha, B., Rientjes, T., Gieske, A. & Haile, A., 2009. Assessment of climate change impacts on the hydrology of Gilgel Abay catchment in Lake Tana basin, Ethiopia. *Hydrological Processes: An International Journal*, 23(26), 3661-3669.

Ahmad, M., Arshad, M., Iqbal, M., Waqas, M.M. & Awais, M., 2017. Simulation of groundwater quantity using hydrological model for Mithawan spate irrigated area of Dera Ghazi Khan, Pakistan. *Pakistan Journal of Agricultural Sciences*, 54(4).

Arshad, A., Mirchi, A., Samimi, M. & Ahmad, B., 2022. Combining downscaled-GRACE data with SWAT to improve the estimation of groundwater storage and depletion variations in the Irrigated Indus Basin (IIB). *Science of the Total Environment*, 838, 156044.

Ashraf, S., Ali, M., Shrestha, S., Hafeez, M.A., Moiz, A. & Sheikh, Z.A., 2022. Impacts of climate and land-use change on groundwater recharge in the semi-arid lower Ravi River basin, Pakistan. *Groundwater for Sustainable Development*, 17, 100743.

Bordbar, M., Rezaie, F., Bateni, S.M., Jun, C., Kim, D., Busico, G., Kardan Moghadam, H., Paryani, S., Panahi, M. & Valipour, M., 2023. Global Review of Modification, Optimization, and Improvement Models for Aquifer Vulnerability Assessment in the Era of Climate Change. *Current Climate Change Reports*, 9, 45–67.

Brouyère, S., Carabin, G. & Dassargues, A., 2004. Climate change impacts on groundwater resources: modelled deficits in a chalky aquifer, Geer basin, Belgium. *Hydrogeology Journal*, 12, 123-134.

Busuioc, A., Giorgi, F., Bi, X. & Ionita, M., 2006. Comparison of regional climate model and statistical downscaling simulations of different winter precipitation change scenarios over Romania. *Theoretical and Applied Climatology*, 86, 101-123.

Çelik, R., 2015. Temporal changes in the groundwater level in the Upper Tigris Basin, Turkey, determined by a GIS technique. *Journal of African Earth Sciences*, 107, 134-143.

Chou, C., Chiang, J. C. H., Lan, C.-W., Chung, C. H., Liao, Y. C., Lee, C. J., 2014. Increase in the range between wet and dry season precipitation. *Nature Geoscience*, 6(4), 263–267.

Chu, J., Xia, J., Xu, C.Y. & Singh, V., 2010. Statistical downscaling of daily mean temperature, pan evaporation and precipitation for climate change scenarios in Haihe River, China. *Theoretical and Applied Climatology*, 99, 149-161.

Collins, M., Knutti, R., Arblaster, J., Dufresne, J. L., Fichefet, T., Friedlingstein, P. & Wehner, M., 2013. Long-term climate change: Projections, commitments, and irreversibility. *In Climate Change 2013: The Physical Science Basis. Contribution of Working Group I to the Fifth Assessment Report of the Intergovernmental Panel on Climate Change* (pp. 1029–1136). Cambridge University Press.

Cui, Y., Liao, Z., Wei, Y., Xu, X., Song, Y. & Liu, H., 2020. The response of groundwater level to climate change and human activities in Baotou City, China. *Water*, 12(4), 1078.

Diancoumba, O., Toure, A., Keita, S., Konare, S., Mounir, Z.M. & Bokar, H., 2023. Predicting groundwater level using climate change scenarios in the southern part of Mali. *American Journal of Climate Change*, 12(1), 21-38.

Gharbia, S.S., Aish, A. & Pilla, F., 2015. Modelling potential impacts of climate change on groundwater of the Gaza coastal aquifer from ensemble of global climate model projections. *Civil and Environmental Research*, 7(2), 44-60.

Goodarzi, M., Abedi-Koupai, J. & Heidarpour, M., 2019. Investigating impacts of climate change on irrigation water demands and its resulting consequences on groundwater using CMIP5 models. *Groundwater*, 57(2), 259-268.

Hempel, S., Frieler, K., Warszawski, L., Schewe, J. & Piontek, F., 2014. A trend-preserving bias correction – The ISIMIP approach. *Earth System Dynamics*, 4(2), 219–236.

Izady, A., Davary, K., Alizadeh, A., Ziaei, A.N., Alipoor, A., Joodavi, A. & Brusseau, M.L., 2014. A framework toward developing a groundwater conceptual model. *Arabian Journal of Geosciences*, 7, 3611-3631.

Khan, M.S., Coulibaly, P. & Dibike, Y., 2006. Uncertainty analysis of statistical downscaling methods using Canadian Global Climate Model predictors. *Hydrological Processes: An International Journal*, 20(14), 3085-3104.

Kowsar, S., 2006. An empirical design of stilling basins for the artificial recharge of groundwater. Paper presented at the Management of aquifer recharge and water harvesting in arid and semi-arid regions of Asia. *Proc. Reg. Workshop held in Yazd, IR Iran, under the auspices of UNESCO*.

Knutti, R. & Sedláček, J., 2013. Robustness and uncertainties in the new CMIP5 climate model projections. *Nature Climate Change*, 3(4), 369–373. https://doi.org/10.1038/nclimate1716

Mahjouri, N., Ghazban, F. & Ardestani, M., 2005. Groundwater quantity and quality management: a case study of Kashan aquifer, central Iran. *Impacts of Global Climate Change*, 1-10.

Mastrocicco, M., Boz, B., Colombani, N., Carrer, G., Bonato, M. & Gumiero, B., 2014. Modelling groundwater residence time in a sub-irrigated buffer zone. *Ecohydrology*, 7(3), 1054-1063.

McDonald, M.G. & Harbaugh, A.W., 1988. A modular three-dimensional finite-difference groundwater flow model. *U.S. Geological Survey*.

Mirzavand, M., Ghasemieh, H., Sadatinejad, S.J. & Bagheri, R., 2020. Delineating the source and mechanism of groundwater salinization in crucial

declining aquifer using multi-chemo-isotopes approaches. *Journal of Hydrology*, 586, 124877.

Mirzavand, M., Sadatinejad, S.J. & Kardan Moghaddam, H., 2025. Spatio-Temporal Optimization of Long-term Groundwater Monitoring Networks Using PSO Algorithm. *Sustainable Earth Trends*, 5(1), 1-12.

Najafi, S., Sharafati, A. & Kardan Moghaddam, H., 2023. Impact of climate change adaptation strategies on groundwater resources: a case study of Sari-Neka coastal aquifer, Northern Iran. *Environmental Earth Science*, 82, 571.

Narany, T.S., Aris, A.Z., Sefie, A. & Keesstra, S., 2017. Detecting and predicting the impact of land use changes on groundwater quality, a case study in Northern Kelantan, Malaysia. *Science of the Total Environment*, 599, 844-853.

Rayne, T.W., Bradbury, K.R. & Muldoon, M.A., 2001. Delineation of capture zones for municipal wells in fractured dolomite, Sturgeon Bay, Wisconsin, USA. *Hydrogeology Journal*, 9, 432-450.

Schweizer, B., 2015. *Darcy's law and groundwater flow modelling*. https://doi.org/10.14760/SNAP-2015-007-EN.

Taie Semiromi, M. & Koch, M., 2020. How do gaining and losing streams react to the combined effects of climate change and pumping in the Gharehsoo River Basin, Iran? *Water Resources Research*, 56(7), e2019WR025388.

Wang, Q., Zhan, H. & Tang, Z., 2014. A new package in MODFLOW to simulate unconfined groundwater flow in sloping aquifers. *Groundwater*, 52(6), 924-935.

Watterson, I. G., Webb, L., Bhend, J. & Hennessy, K., 2015. Changes in precipitation seasonality and extremes in a global warming scenario. *Climate Dynamics*, 45(3-4), 853–872.

Wilby, R.L., Wigley, T., Conway, D., Jones, P., Hewitson, B., Main, J. & Wilks, D., 1998. Statistical downscaling of general circulation model output: A comparison of methods. *Water Resources Research*, 34(11), 2995-3008.

Wilby, R.L. & Wigley, T.M., 1997. Downscaling general circulation model output: A review of methods and limitations. *Progress in Physical Geography*, 21(4), 530-548.

Wu, C., Huang, G. & Yu, H., 2015. Prediction of extreme floods based on CMIP5 climate models: A case study in the Beijiang River basin, South China. *Hydrology and Earth System Sciences*, 19(3), 1385-1399.

Yidana, S.M., Vakpo, E.K., Sakyi, P.A., Chegbeleh, L.P. & Akabzaa, T.M., 2019. Groundwater–Lake water interactions: an evaluation of the impacts of climate change and increased abstractions on groundwater contribution to the Volta Lake, Ghana. *Environmental Earth Sciences*, 78, 1-16.

Zhou, Y. & Li, W., 2011. A review of regional groundwater flow modeling. *Geoscience Frontiers*, 2(2), 205-214.